Physical Approach to Ferroelectric Impedance Spectroscopy: The Rayleigh Element

T. Schenk,[1,a,*] M. Hoffmann,[1] M. Pešić,[1] M. H. Park,[1] C. Richter,[1] U. Schroeder,[1] and T. Mikolajick[1,2]

[1]*NaMLab gGmbH, Noethnitzer Str. 64, D-01187 Dresden, Germany*

[2]*Chair of Nanoelectronic Materials, TU Dresden, D-01062 Dresden, Germany*

The Rayleigh law describes the linear dependence of the permittivity of a ferroelectric on the applied ac electric field amplitude due to irreversible motions of domain walls. We show that this gives rise to a new equivalent-circuit element predestined to fit the impedance spectra of ferroelectrics based on an accepted physical model. Such impedance spectroscopy is a powerful tool to obtain a dielectric and resistive representation of the entire sample structure. The superiority of the Rayleigh analysis based on impedance spectroscopy compared to the common single-frequency approach is demonstrated for a ferroelectric Si : HfO_2 thin film.

I. INTRODUCTION

Capacitance measurements play a very central role in the investigation of ferroelectric materials as they provide insight into dielectric properties and relaxations: The relative permittivity ϵ_r is related to the crystallographic phase and microstructure of the material and its temperature dependence allows to identify phase transitions, their order, or even relaxor-ferroelectric behavior [1,2]. Bias field-dependent (small-signal or weak-field) measurements of ϵ_r show a butterfly-shaped characteristic with enhancements close to the coercive fields stemming from domain wall contributions [3]. For subcoercive fields, a linear increase of the permittivity with increasing ac excitation field amplitude is observed if the material obeys what is called Rayleigh behavior [3–6]. This increase is related to an increasing motion or displacement of pre-existing domain walls as an extrinsic contribution to the dielectric and piezoelectric behavior [3,5–8]. The interaction of the moving domain walls with obstacles that form a random energy profile gives rise to the Rayleigh behavior as has been derived theoretically [9–11]. In the following, it will be shown that this Rayleigh behavior has implications for impedance spectroscopy. A new equivalent-circuit element, called the "Rayleigh element," will be derived. Moreover, the importance and superiority of using a wide frequency range compared to a single-frequency approach will be stressed and demonstrated

using the example of a ferroelectric thin-film capacitor based on Si:HfO_2.

II. RAYLEIGH BEHAVIOR AND RAYLEIGH ANALYSIS

Figure 1 shows a simplified physical schematic of the origin of Rayleigh behavior and the corresponding experimental observations in small-signal capacitance measurements. The relative permittivity increases linearly once the applied excitation field E_0 exceeds a certain threshold field and the domain wall or boundary can move across the present landscape of potential energy [3,9,12]. This landscape depends on the environment of the boundary, namely the crystallographic phase and composition as intrinsic contributions as well as grain size, defects, and their distribution as extrinsic contributions [3]. Ideally, if the domain wall only moves reversibly in a harmonic-oscillator-like potential, only linear dielectric behavior is observed, i.e., a straight line in the graph of polarization P vs electric field E. With the potential not exhibiting the parabola shape of the harmonic oscillator, this line can become nonlinear, but stays nonhysteretic. This is still referred to as a reversible contribution to the dielectric behavior and is impacted by both intrinsic and extrinsic factors. Only if the excitation field is large enough to make the domain wall move irreversibly, i.e., also outside its original potential well, are a hysteresis and an increase in relative permittivity observed. Appendix B explains that this situation is a special case of the Preisach model [13]. The slope $d\epsilon_r/dE_0$ and the linearly extrapolated ϵ_r-axis intercepts of this so-called Rayleigh plot represent the Rayleigh constant and the reversible relative permittivity (intrinsic and reversible

───────────

[a]Currently at Materials Research and Technology Department, Luxembourg Institute of Science and Technology (LIST), 41 Rue du Brill, Belvaux, Luxembourg.
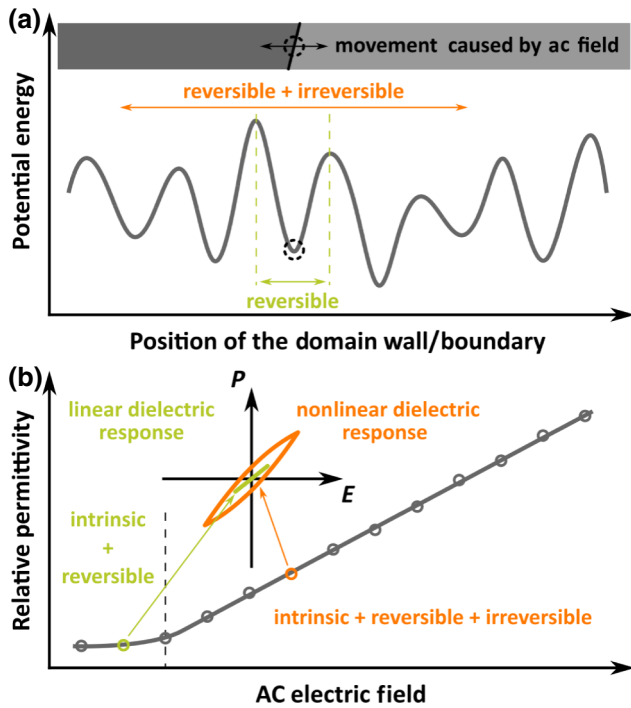
[*]tony.schenk@list.lu

FIG. 1. Simplified sketch of the origin and manifestation of Rayleigh behavior. (a) Domain walls/boundaries move in a random energy landscape when subjected to an ac electric field. (b) Depending on the amplitude of this excitation field, the measured small-signal permittivity stems either only from reversible or also from irreversible contributions. The latter is caused by the movements of walls/boundaries extending outside their original local energy minima instead of just oscillating within their original local potential well. Compare Refs. [3] and [36].

extrinsic contributions) of the material. As they are a consequence of the energy landscape of the moving boundary, they can be impacted by changes in sample composition or preparation [9,14,15]. Moreover, monitoring the evolution of these properties can give insights into initial structural changes or degradation mechanisms leading to fatigue during field cycling as a lifetime concern in applications such as ferroelectric memories [3,15].

It has been shown that not only the real part of permittivity follows a linear relationship, but also the imaginary part describing the losses increases linearly as a consequence of the occurrence of a subloop hysteresis [5]. The corresponding Rayleigh formulas of the real and imaginary parts of the relative permittivity are given by

$$\varepsilon_r' = \varepsilon_{r,\mathrm{in}}' + \alpha E_0 \qquad (1)$$

and

$$\varepsilon_r'' = \varepsilon_{r,\mathrm{in}}'' + \frac{4}{3\pi}\alpha E_0, \qquad (2)$$

respectively [5,6]. Here, E_0 is the ac field amplitude, α is the Rayleigh constant, and $\varepsilon_{r,\mathrm{in}}'$ and $\varepsilon_{r,\mathrm{in}}''$ represent the

reversible values of the real and imaginary parts of ϵ_r. Note that $\varepsilon_{r,\mathrm{in}}'$ is related to capacitive contributions while $\varepsilon_{r,\mathrm{in}}''$ is related to resistive contributions to the impedance.

Publications utilizing these methods often only present permittivity data obtained from single frequencies, e.g., 1, 10, or 100 kHz to name a few typical frequencies. These frequencies are far away from the microwave or infrared range where ionic (fixed particle in a crystalline lattice not space-charge polarization, which is also sometimes referred to as "ionic") or atomic relaxations occur [16]. Nonetheless, the frequency range plays a crucial role if the dielectric and resistive properties of the sample are not homogeneous. Grain boundaries or segregations are prominent examples of inhomogeneities in ceramic samples [16,17]. For thin films, which are exemplarily used in this work, interfacial layers become more and more important as the thickness ratio of "bulk" and interface decreases. Measuring the complex quantity of impedance as the generalized ac resistance of a sample over a certain frequency range (usually several orders of magnitude) allows fitting of an equivalent circuit to the extracted impedance spectrum. The elements of this circuit represent resistive, capacitive, and inductive contributions from the different physical components that form the sample, such as electrodes, interfaces, bulk, or even different phases within the bulk. A recent study on capacitors made of 27-nm-thin Gd:HfO$_2$ sandwiched between TiN electrodes showed that for frequencies above 1 kHz, the impedance is dominated by the interfacial properties [18]. Resistive or capacitive values extracted at a single frequency in that range are by no means a reflection of the ferroelectric bulk properties. Thus, using these values to distinguish different known polymorphs of the material to perform a Rayleigh analysis to assess domain wall contributions or to check for phase transitions in temperature-dependent plots of the permittivity might result in misleading interpretations. It should be noted that this is a major difference to bulk samples (compare Appendix C). For bulk samples with grain boundaries parallel to the electrodes, the situation often is the other way around: The lower frequency range might be dominated by the grain boundaries while the bulk properties can only be obtained from the impedance characteristics for higher frequencies [19]. As a consequence, a proof of the suitability of the chosen frequency by impedance analysis is mandated prior to every extraction based on a single-frequency approach.

III. IMPEDANCE SPECTROSCOPY AND DERIVATION OF AN EQUIVALENT-CIRCUIT ELEMENT BASED ON THE RAYLEIGH LAW

In the present work, a Rayleigh analysis based on impedance spectroscopy is demonstrated. This approach has the advantage of being free of artifacts from an unfortunate choice of the measurement frequency and provides a

statistically more reliable parameter extraction. Moreover, some similarities and differences between the Rayleigh element and another frequently used equivalent-circuit element, the so-called "constant-phase element," are pointed out. As different sign conventions are used, we start defining the complex quantities of impedance Z and admittance $Y = 1/Z$ with their real (single-primed symbol) and imaginary parts (double-primed symbols) as

$$Z = Z' - iZ'' \qquad (3)$$

and

$$Y = Y' + iY'', \qquad (4)$$

respectively. For the sake of convenience, we only use the admittance equations in the following. The circuit element of a perfect resistance R is defined as

$$Y = Y' + iY'' = \frac{1}{R} \qquad (5)$$

and a perfect capacitance C is given by

$$Y = Y' + iY'' = i\omega C. \qquad (6)$$

In Eqs. (2)–(6), i is the imaginary unit and ω is the angular frequency and is given by $\omega = 2\pi f$, where π is the Archimedes constant and f is the frequency [17]. The capacitance C in a parallel-plate capacitor can be calculated from the plate area A, plate distance d, the relative permittivity ϵ_r, and the electric field constant ϵ_0 as

$$C = \varepsilon_0 \varepsilon_r \frac{A}{d}. \qquad (7)$$

In some cases, fits with a perfect capacitance do not succeed and a so-called "constant-phase element" (CPE) is used instead [17]. Its impedance and admittance are given by

$$Y = Y' + iY'' = T(i\omega)^n$$
$$= T\omega^n \left[\cos\left(n\frac{\pi}{2}\right) + i\sin\left(n\frac{\pi}{2}\right) \right]. \qquad (8)$$

Here, T is often referred to as the pseudo-capacitance and n is both the exponent of $(i\omega)$ and the prefactor of $\pi/2$ defining the phase angle φ in the cosine and sine expressions. This phase angle is constant, and with it the ratio of imaginary and real parts of Z and Y, hence the name CPE [17]. This is also a central property of the formulas for what has been called the "universal dielectric response" and the CPE is one possible representation of this type of response (compare Appendix B). For $n = 1$ and for $n = 0$, the CPE equals a perfect capacitance and resistance, respectively. All intermediate cases $1 > n > 0$ give rise to finite capacitive and resistive contributions of the CPE.

This makes the CPE very flexible and thus, a frequently used element to fit imperfect capacitive behavior. However, extracting physically meaningful material parameters from such a fit is challenging without a very reliable model in mind [17]. Existing explanations include film roughness [17] as well as inhomogeneities in resistivity and/or permittivity (distributed in-plane and/or normal to it) [20–25]. In the following, it will be shown that similar, but slightly different behavior can be explained solely based on the empirical Rayleigh law.

Coming back to the Rayleigh formulas, Eqs. (1) and (2), we see that these equations have similar implications for the expected impedance spectra. If both $\varepsilon''_{r,\mathrm{in}}$ and α are not nearly equal to zero, the ferroelectric exhibits a certain resistive component and the ratio of the imaginary and real parts is independent of the measurement frequency. This ratio and with it the exponent n is given by

$$\tan\left(n\frac{\pi}{2}\right) = \frac{Y''}{Y'} = \frac{\varepsilon'_r}{\varepsilon''_r} = \frac{\varepsilon'_{r,\mathrm{in}} + \alpha E_0}{\varepsilon''_{r,\mathrm{in}} + \frac{4}{3\pi}\alpha E_0}. \qquad (9)$$

In Eq. (10), n is no longer required as the exponent of both i and ω, but instead only defines the phase angle as i^n. Consequently, this element has the same frequency dependence as a normal capacitance. The resulting equivalent-circuit element will be called the "Rayleigh element" in the following and its admittance for a parallel-plate geometry as in Eq. (7) are given in analogy to the notations in Eq. (8) by

$$Y = Y' + Y'' = i^n \omega |C| = \omega\varepsilon_0 \frac{A}{d}[\varepsilon''_r + i\varepsilon'_r]$$
$$= \omega\varepsilon_0 \frac{A}{d}\left[\left(\varepsilon''_{r,\mathrm{in}} + \frac{4}{3\pi}\alpha E_0\right) + i(\varepsilon'_{r,\mathrm{in}} + \alpha E_0)\right]. \qquad (10)$$

Here, $|C|$ indicates the absolute value of the complex capacitance given by the real and imaginary contributions of the relative permittivity. Impedance spectroscopy allows to fit $|C|$ and n. The reversible relative permittivities and the Rayleigh constant, however, cannot be obtained from a measurement with a single ac field amplitude E_0 alone. Similar to the Rayleigh analysis based on a single frequency, the impedance spectroscopy-based approach also relies on measurements at different E_0. The basic equivalent-circuit elements in Eqs. (5) and (6) obey the Kramers-Kronig (KK) relation, which is often used to check whether measurement data are free of artifacts. A discussion of the applicability of the KK relation can be found in Appendix D, while the limitations of treating the Rayleigh element within the frame of linear perturbation theory are discussed in Appendix B.

Before continuing with the practical application of these equations, some remarks should be made. Here, we choose the simplest form of nonlinearity reported for ferroelectric materials. We would like to also stress

that other approaches exist, which represent an extension of the simplest form of the Rayleigh model chosen here in this initial demonstration of the concept. They are based, e.g., on a power series [26], polynomials [27], or hyperbolic laws [28] to describe the dependence of small-signal permittivity from the applied ac field amplitude. Additional frequency dependences of the Rayleigh parameters can also be introduced and accounted for if desired [8,29–31]. There is no single best choice among the above approaches. They can be implemented in a separate equivalent-circuit element in a similar way. The choice depends on the dominating effects in the sample to be characterized. If both the impedance spectra and the resulting Rayleigh plots can be modelled properly, the model can be considered a valid representation of reality.

IV. PRACTICAL DEMONSTRATION OF RAYLEIGH ANALYSIS BASED ON IMPEDANCE SPECTROSCOPY

In the following, the corresponding analysis is demonstrated for a ferroelectric thin-film capacitor based on 40-nm-thick Si:HfO$_2$ with TiN electrodes fabricated on a Si substrate similar to what has been described elsewhere [32]. Further details including basic electrical and structural data evidencing the antiferroelectric character (field-induced phase transition) of the sample can be found in Appendix A. Impedance analysis is performed as explained in section S1 within the Supplemental Material [33,34]. Figure 2 exemplarily shows the fit results for $E_0 = 17.7$ MV/m ($=0.5$ V rms) including the parameters of the utilized equivalent circuit. The corresponding results and fit parameters for all other values of E_0 are provided in section S1 within the Supplemental Material [34] for completeness. Figure 2 consists of different plots that highlight different frequency ranges of the impedance spectrum. The logarithmic Bode-plots of impedance and admittance in Figs. 2(a) and 2(b) give an overview of the fit results for the full spectrum. The (linear) Bode-plots in Figs. 2(c) and 2(d) and the Cole-Cole plot of the admittance in Fig. 2(f) show the intermediate as well and the higher-frequency range ($f > 1$ kHz) in more detail, while Fig. 2(e) gives a better insight into the fit for $f < 1$ kHz. To get an insight into the accuracy of the fitted model over the frequency spectrum, the sign-corrected and amplitude-weighted square errors Δ are given in Fig. 2(g). Finally, the utilized equivalent circuit is shown in Fig. 2(h). The series resistance R_3 corresponds to imperfect electrode layers, the RC-like element consisting of R_2 and a CPE is attributed to an interfacial layer adjacent to the TiN electrodes, while the RC-like element formed by R_1 and the Rayleigh element represents the ferroelectric bulk following the explanation previously presented by Grimley and Schenk *et al.* [18].
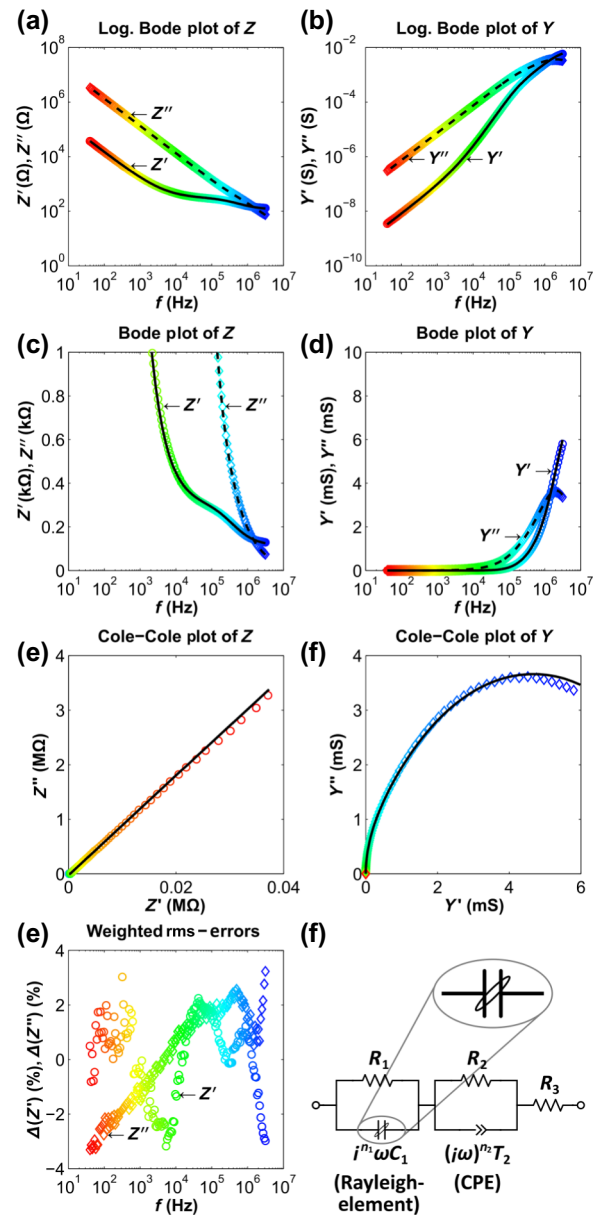

FIG. 2. (a) Impedance Z and (b) admittance Y in logarithmic Bode plots give a rough overview of the fit quality for the whole frequency spectrum. The linear Bode plots in (c) and (d) and the Cole-Cole plot of the admittance in (f) give more detailed insight into the higher frequency range whereas the Cole-Cole plot of impedance in (e) proves a high fit quality in the frequency range below 1 kHz. (g) Square errors Δ of Z' and Z''. The employed equivalent circuit including a proposed symbol of the Rayleigh element formed by a capacitor with an overlaid stylized Rayleigh loop in (h). $E_0 = 17.7$ MV/m ($=0.5$ V rms); Fit curves are shown as black solid lines, open symbols represent measured data, with the color decoding the frequency as can be seen from (a)–(d).

Next, ε_r' and ε_r'' are calculated following Eq. (10) from the fit parameters of the Rayleigh element ($|C|$ and n) for the different values of E_0. The corresponding values of ε_r' and ε_r'' as a function of E_0 are shown in Fig. 3(a). From

this Rayleigh plot, the parameters $\varepsilon'_{r,\text{in}}$, $\varepsilon''_{r,\text{in}}$, and α can be extracted according to Eqs. (1) and (2) as the intercepts of a linear fit with the y axis. With 2.37, the ratio of the two slopes, $d\varepsilon''_r/dE_0$ to $d\varepsilon'_r/dE_0$, is in very good agreement with the theoretical value of $3\pi/4 \approx 2.36$ mandated by the Rayleigh law. The measured values deviate from the linear trend for the lowest two E_0 similar to what has been observed for conventional perovskite-based ferroelectric ceramics and thin films [5,9,29]. It is related with the existence of a so-called threshold field that has to be overcome to see the manifestation of domain wall contributions to the measured relative permittivity. Moreover, values of $\varepsilon'_{r,\text{in}} = 35.4$, $\varepsilon''_{r,\text{in}} = 0.33$, and $\alpha = 7.0 \times 10^{-9}$ m/V are obtained. The values match quite well with those reported in a previous study on similar ferroelectric TiN-Si:HfO$_2$-TiN capacitors with a hafnia thickness of 10 nm: Guan *et al.* [35] obtained values of $\varepsilon'_{r,\text{in}} = 44$–$47$, $\varepsilon''_{r,\text{in}} = 0.41$, and $\alpha = (8-13) \times 10^{-9}$ m/V for the

temperature range of $T = 120$–300 K and using slightly higher fields from 0.125 to 0.6 MV/cm. Compared to Rayleigh constants between approximately 10^{-5} and 10^{-2} m/V measured in conventional ferroelectrics [5,15, 36,37], the Rayleigh constants for hafnia-based ferroelectrics are at around 3 orders of magnitude smaller. This means that the domain boundary or interphase boundary movement [38] is much harder. Given that the relative permittivity of hafnia is one to 2 orders of magnitude smaller than typical values for lead zirconate titanate, i.e., a displacement of ions by an electric field is more difficult anyway, so at least the trend is not surprising. Moreover, it fits the observation of a 2 orders of magnitude lower lateral-domain-wall velocity compared to lead zirconate titanate by piezoresponse force microscopy analysis [39]. The prominent interphase boundaries reported by Grimley *et al.* [38] might also account for this. Another way to check the consistency with Rayleigh behavior is shown in Fig. 3(b). From this plot of ε'_r against ε''_r, a slope of 2.37 is extracted, which again matches very well with the theoretical value of 2.36. Moreover, extrapolating the linear region to $\varepsilon''_r = 0$, the so-called "zero-loss" value of $\varepsilon'_r = 34.6$ can be extracted as the ε'_r-axis intercept. The reversible relative permittivity, i.e., the extrapolation of ε'_r in the Rayleigh plot in Fig. 3(a) to zero field, represents the quantity without irreversible domain-wall movement across a random potential landscape formed by pinning centers [3,12,36]. In contrast, the physical meaning of the zero-loss value is the relative permittivity of the ferroelectric material without the presence of any reversibly vibrating domain walls or phase boundaries (within their current potential minimum) [30]. This value could be of interest for comparisons to theoretical values or values measured on single crystals. However, the present films are polycrystalline and the obtained quantity is an average according to the texture of the thin film, which, moreover, could contain nonferroelectric phase fractions as Fig. 2(b) suggests. The fact that the imaginary reversible value of ε''_r is not zero could be an indication of an internal bias [27] or stress fields [40]. Both have been reported in similar samples [41–43].

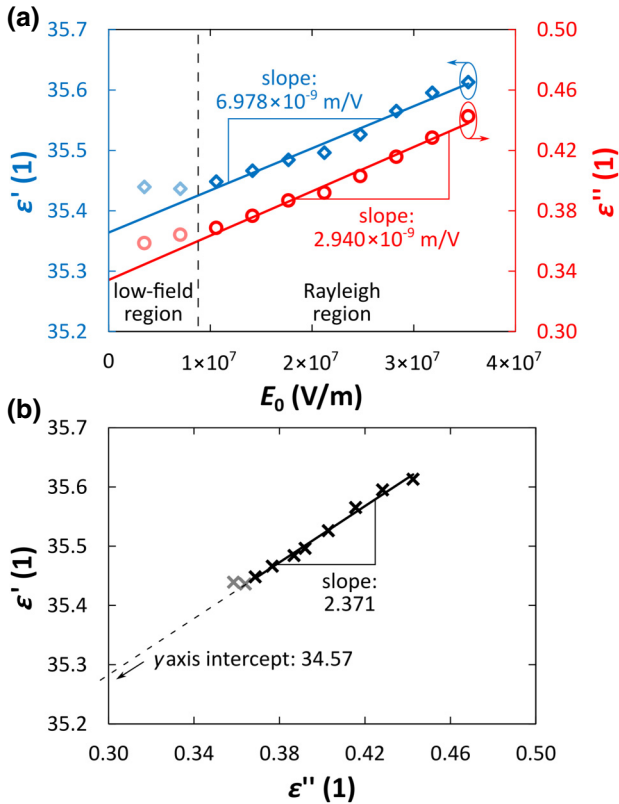FIG. 3. (a) Rayleigh plots of the real and imaginary parts of the relative permittivity ε_r. The slopes allow the extraction of the Rayleigh constant α, while the y intercepts represent the reversible values $\varepsilon'_{r,\text{in}}$ and $\varepsilon''_{r,\text{in}}$. (b) Cole-Cole-like plot of the real and imaginary parts of ε_r. The slope in this plot represents the slope ratio of the two Rayleigh plots in (a) and the y intercept is called (relative) "zero-loss permittivity." The high quality of all linear fits in (a) and (b) is evidenced by coefficients of determination of $R^2 > 0.975$. A complementary plot of $\tan(\varphi)$ vs E_0 is given in the section S2 within the Supplemental Material [34].

V. COMPARISON TO SINGLE-FREQUENCY APPROACHES OF RAYLEIGH ANALYSIS

To demonstrate the advantages of this impedance spectroscopy-based approach, Rayleigh plots for single frequencies are shown in section S3 within the Supplemental Material [34]. It can be seen that the linear trends are not as smooth as in Fig. 3(a). Table I summarizes the values for $\varepsilon'_{r,\text{in}}$, $\varepsilon''_{r,\text{in}}$, α, and slope ratios $d\varepsilon''_r/dE_0$ to $d\varepsilon'_r/dE_0$ extracted from the impedance and the single-frequency-based approaches for frequencies ranging from 105 Hz to 1.03 MHz. For 105 Hz, the values are in a similar range as the ones obtained from the impedance fits despite the

TABLE I. Comparison of Rayleigh constants, reversible properties, and slope ratios derived from Rayleigh analysis based on impedance analysis and single-frequency measurements.

Approach for Rayleigh analysis	$\varepsilon'_{r,\text{in}}$	$\varepsilon''_{r,\text{in}}$	α in 10^{-9} cm/MV	$(d\varepsilon''_r/dE_0)/(d\varepsilon'_r/dE_0)$
Full impedance fit with Rayleigh element	35.4	0.33	14.0	2.37
Single-frequency: 105 Hz	36.1	0.36	10.6	3.29
Single-frequency: 1.04 kHz	36.0	0.44	1.5	0.61
Single-frequency: 10.4 kHz	35.1	1.16	4.8	1.92
Single-frequency: 103 kHz	32.3	6.61	5.7	1.35
Single-frequency: 1.03 MHz	14.8	11.80	−0.2	−0.06

strong deviation from a linear trend and the fact that the slope ratio is 3.29 instead of 2.36 as demanded by Rayleigh law. For higher frequencies, the discrepancies rise significantly. The value of $\varepsilon'_{r,\text{in}}$ stays nearly constant when going from 105 Hz to 1.04 kHz, but after 10.4 kHz, it starts decreasing drastically as the parasitic losses given by $\varepsilon''_{r,\text{in}}$ start exceeding an absolute value of 1. Moreover, the mismatch between the slope ratio $d\varepsilon''_r/dE_0$ to $d\varepsilon'_r/dE_0$ proves that the Rayleigh model obviously cannot be applied here. The observed losses have nothing to do with the losses stemming from domain-wall motion as inferred by the Raleigh law. The impedance fit suggests they have to be attributed to the resistive behavior of the interfacial layer and the (nonperfect) electrodes similar to what has been done for a comparable film stack elsewhere [18,44]. Extracting parameters in this frequency range, thus, cannot give insights into the ferroelectric bulk properties.

VI. CONCLUSION

In conclusion, this work demonstrates two major aspects. First, an equivalent-circuit element follows directly from Rayleigh law and is consequently called a "Rayleigh element." It is successfully used to fit impedance spectra for a 40-nm-thin Si:HfO$_2$ film. Second, it is pointed out that not any arbitrarily chosen frequency range is suitable to obtain the properties of the ferroelectric bulk and a careful check of the impedance spectrum is inevitable. Moreover, an approach of Rayleigh analysis based on impedance analysis and the new Rayleigh element is presented. The linear relations found in the Rayleigh plots evidence the self-consistency of the model as they show the validity of the presumptions for the derivation of the Rayleigh element used to fit the impedance spectra. The advantages of this approach compared to the conventional single-frequency method are proven and the risks of such a single-frequency approach are shown in practice. This work is intended to serve as a guideline for future work on thin films, but also for thicker films and ceramics. In the field of ferroelectric hafnia and zirconia films, it paves the way toward comparisons of the true bulk properties and domain-related losses for a variety of samples. Those studies to come could include different dopants, film thicknesses, and annealing and/or fabrication parameters as well as fatigue and wake-up behavior. Moreover, the Rayleigh element can be extended by incorporating more complex laws to represent the expected mechanisms of the respective studied sample even more accurately. The discussed superiority of the presented approach based on impedance spectroscopy compared to a single-frequency measurement and the need to carefully check the frequency range, however, remains unaffected.

APPENDIX A: BASIC ELECTRICAL AND STRUCTURAL DATA FOR THE USED FERROELECTRIC CAPACITOR

The fabrication of the stack shown in the inset of Fig. 4(a) was described previously [32]. A 10-min-long anneal in nitrogen atmosphere at 800 °C is used to crystallize the ferroelectric. Figure 4(a) shows the polarization hysteresis obtained using an aixACCT TF Analyzer 3000 and a frequency of 1 kHz and with a sinusoidal waveform of the excitation voltage. A clear double loop hints on the field-induced phase transformation from a nonpolar tetragonal to the polar orthorhombic phase [32,45]. Although the saturation region shows slight rounding, leakage becomes prominent only at even higher field amplitudes. A rounded shape is present for the lower field amplitudes as well
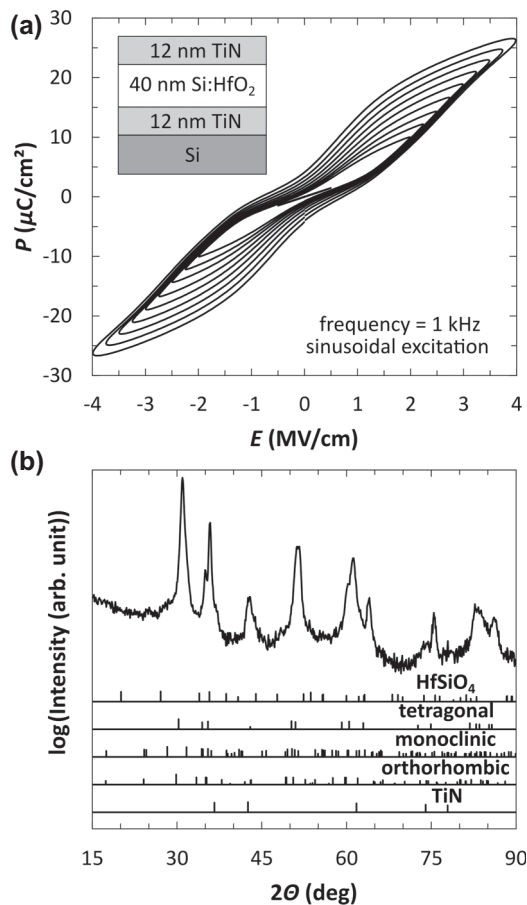
FIG. 4. (a) Polarization hystereses for different electric field amplitudes. The inset shows the capacitor stack consisting of 40-nm Si : HfO$_2$ sandwiched between 12-nm-thick TiN electrodes. (b) Grazing-incidence x-ray diffractogram showing the prominent tetragonal hafnia phase (powder diffraction file no.: 04-011-8820).

and is only due to the sinusoidal excitation. However, the hysteresis does not close completely at zero field. This is not primarily due to ferroelectric phase fractions, but rather stems from the presence of a certain distribution in the internal bias fields as shown earlier [46–48]. From the grazing-incidence x-ray diffractogram (Bruker D8 Discover, Cu K_α: 0.154-nm wavelength) shown in Fig. 4(b), the typical indications [32] of this tetragonal phase at zero field can be seen. Only minor fractions of secondary phases (monoclinic or orthorhombic hafnia or HfSiO$_4$) are present as evidenced by the small intensity peak at $2\Theta = 35°$.

APPENDIX B: APPLICABILITY OF LINEAR PERTURBATION THEORY AND RELATION WITH UNIVERSAL DIELECTRIC RESPONSE AND THE PREISACH MODEL

The basis of Rayleigh behavior is a linear change of the relative permittivity with the applied ac field amplitude.

This automatically means there is no linearity of the dielectric response, i.e., the relation of polarization and the electric field. However, this permittivity is still considered a small-signal (also weak-field or low-field) response [3,5, 6,16,36] as the applied fields are below the coercive fields of the ferroelectric and no permanent switching occurs. The Rayleigh equation gives the same response for every subsequent ac field cycle at constant amplitude, which means it is not history dependent and can be considered steady-state in contrast to what happens proceeding above the coercive fields toward the large-signal *P-E* hysteresis. So, in that sense, the approach is beyond the strictly linear perturbation theory. But this is the case for any analysis where a resistor is used to represent current flow through a dielectric bulk or grain boundaries [49,50]. It is, therefore, quite common to use the term impedance spectroscopy in that wider sense.

As linearity is only approximately rather than perfectly fulfilled, the question might arise as to whether Kirchhoff's laws [51] (which can be also derived from Maxwell's laws [52,53]) are obeyed or not. The answer is that non-linearity, even to a large extent, does not impair the applicability of Kirchhoff's laws. They are obeyed if the equivalent-circuit elements have a nonlinear characteristic (e.g., a diode). Kirchhoff's laws stem from (1) the conservation of charge and (2) the conservation of electrostatic energy. Therefore, they are also true in nonlinear circuits. The criterion of linearity does not play a role in these laws. If nonlinearity impaired them, the Sawyer-Tower circuit, shunt method, and other approaches to measure large-signal hysteresis loops would not work as some important prerequisites would be even less fulfilled than in our only weakly nonlinear system. These set ups rely on the fact that the voltage is divided between two series elements given by the sample and the reference capacitor or resistor and that the displacement current or current flowing through them equals the displacement current through the ferroelectric [54,55]. This means Kirchhoff's laws are the foundation for these approaches, which deal with an even stronger nonlinearity than our circuit element. A more important practical requirement is that every voltage cycle gives the same current response in order to ensure that averaging (similar to what is done in an impedance analyzer) can be applied.

Beyond that, we want to stress that there is some striking similarity between our and the universal dielectric (or dynamic) response, which has been substantially promoted under this term by Jonscher [56–59], but also criticized by others [60]. The main characteristic of the universal dielectric response is a power-law expression for the impedance with a fractal exponent for the angular frequency. Such a dielectric response can be represented by a constant-phase element as pointed out in the main text. As soon as one introduces a nonzero imaginary part of the permittivity, the loop of polarization vs voltage opens and is no

longer a straight line. The loop area corresponds to the lost energy per field cycle [56,61]. This is true whether or not the imaginary and real components of P behave linearly. Jonscher additionally points out that his real and imaginary components scale with the electric field [56]. This description is similar to what the Rayleigh law demands except that the lost energy is scaled quadratically with the electric field in Jonscher's scenario and cubically for the Rayleigh model [5,6]. Jonscher also mentions linearity in his derivations. Nonetheless, it is hard to see from the measured impedance data alone how good the compliance with "linearity" actually is. In practice, there might be a smooth transition between one and the other case.

From Rayleigh law, a representation of P vs E can be derived as

$$P(E) = (\varepsilon_{r,\text{in}} + \alpha E_0)E \mp \frac{\alpha}{2}(E_0^2 - E^2). \qquad \text{(B1)}$$

This is sometimes also called the Preisach hysteresis. However, it is only a special case of what Preisach [13] described. Preisach argues that a macroscopic hysteresis consists of the microscopic contributions of elemental hysteresis, which are called bistable units. These units are characterized with a field for flipping toward positive polarization (switching field) and a field at which they flip toward the negative polarization state (backswitching field). Integration of the probability distribution (switching density) over these fields constitutes the macroscopically measured polarization hysteresis. Equation (B1) only follows for a uniform distribution of switching and backswitching fields. A nonuniform distribution yields different results [41,62,63]. The case of a uniform distribution is usually fulfilled if the maximum fields applied to the sample are significantly lower than the coercive field of the ferroelectric. This situation can be explained well by what is depicted in Fig. 1 in the main text: a random energetic potential [9–11]. It can be shown by Fourier series expansion that Eq. (B1) gives rise to higher harmonics as a result of its nonlinearity. These harmonics are not (or at best only partially depending on the bandwidth) included in the response measured by the impedance analyzer, which represents an inherent limitation to the applicability of this model for significant deviations from linear response theory, which should be kept in mind.

APPENDIX C: DIFFERENCE BETWEEN IMPEDANCE SPECTRA FOR BULK AND THIN-FILM SAMPLES

Impedance spectroscopy is a powerful tool that can help to identify sample regions of different resistive and dielectric properties and attribute them to different physical components of the sample [17]. A textbook example is the discrimination between grains and grain boundaries in electroceramics. Often, two more or less separate

semicircles in the Cole-Cole plot of $-Z''$ vs Z' are found: one at lower frequencies for the grain boundaries and one at higher frequencies for the grains. This observation can be explained by the so-called "brickwork model" [19]. Within this model, the necessary precondition for this observation is that grains and grain boundaries are connected in series. Otherwise, the real and imaginary current flows would only be dominated by the lowest-resistive and highest-capacitive components. This means all grains and grain boundaries in parallel are not distinguishable. To observe the semicircle of the grain boundaries at the lower frequencies, the boundaries need to exhibit a higher resistance than the bulk. However, the resistance should not be more than 1 or 2 orders of magnitude different, else the second arc representing the grains cannot be seen with the unaided eye. Assuming some hundreds of μm- or mm-thick samples with grain sizes on the order of 1 μm, many grains and grain boundaries are passed by the current flowing through the sample. Interfaces toward the electrodes might become effective as well depending on their properties, but might also simply be given by a segregated phase surrounding the grains, similar to the grain boundaries in the rest of the film. Due to their low thickness compared to the bulk, they are expected to allow for large real and imaginary current flows (low resistance, large capacitance), which means that they might not dominate the measured impedance or admittance signal in any frequency range as they are unlikely to be the current-limiting element.

Going from mm-thick ceramics toward films that are only a few tens of nanometers thick, the situation changes. Three main differences are to be considered:

(1) The ratio of interface thickness to bulk thickness changes significantly and the interfaces gain importance. However, the resistance of the interfaces is anticipated to be smaller than the one of the grains and grain boundaries, which means that the respective equivalent-circuit element is dominant at the higher frequency branch when the capacitive current flow through grains and grain boundaries shorts their high resistivity. In contrast to the ceramic sample, the semicircle for the grains is thus found at lower frequencies.

(2) If the grains span the whole film thickness [18,64], as reported for hafnia-based ferroelectric films such as the one used in this work, there are no grain boundaries in series to the grains. Grains and grain boundaries are not separable anymore and the resistive and capacitive components allowing for the largest real and imaginary current flows, respectively, dominate the spectral response.

(3) Finally, grain boundaries possess a much larger conductivity than the bulk as has been shown by conductive atomic force microscopy [65,66]. This means that the grains dominate the capacitive behavior due to the larger area compared to the grain boundaries, while the latter dominate the resistive behavior due to their significantly
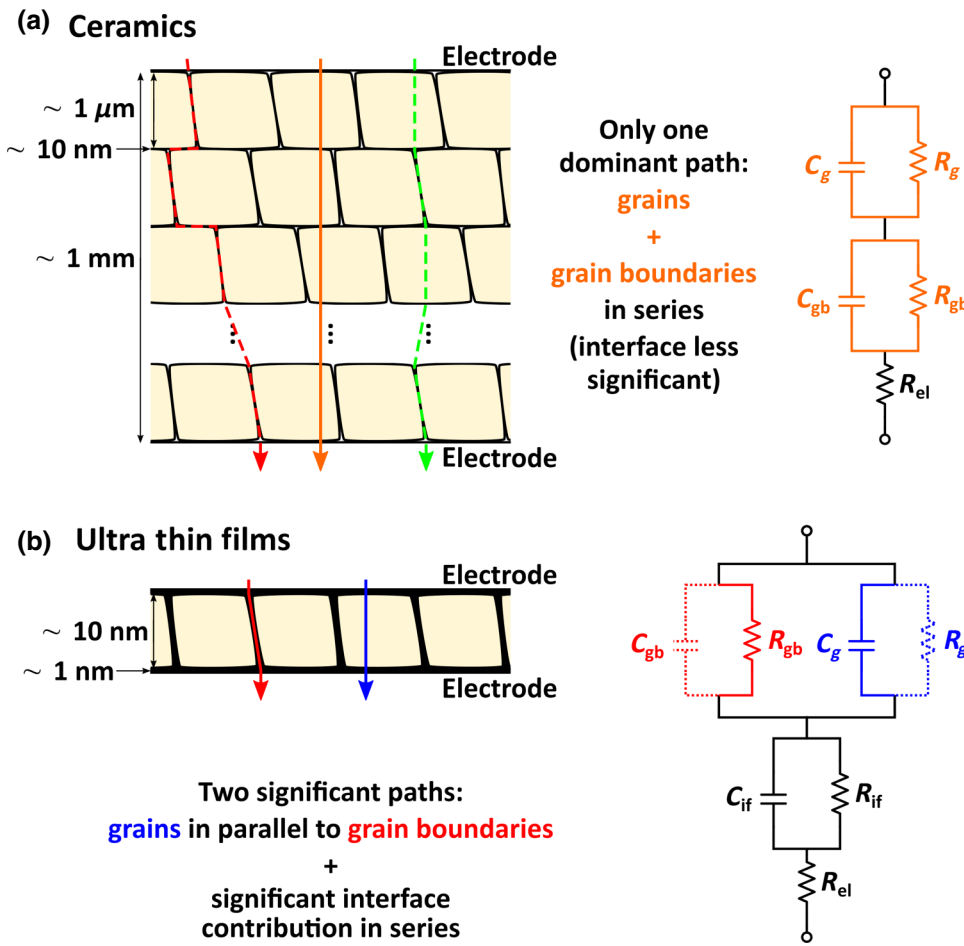
FIG. 5. Illustration of the physical components of (a) a thick-ceramic sample and (b) a thin-film sample with arrows representing current paths. The colors of arrows, text, and circuit elements correspond to each other. The orange current path is the significant one for the thick ceramic and contains an RC element for the grains (index g) and another one for the grain boundaries (index gb) in series. For the thin film (here, especially, what has been found for hafnia), two paths are significant—one via the grains, one via the grain boundaries. Both form a parallel connection and are mathematically inseparable. Therefore, only one component might dominate the resistive and capacitive current contributions. In series to both, there is an interfacial RC element that gains importance as the film thickness reduces.

lower resistance. Nonetheless, it should be kept in mind that grains and grain boundaries are mathematically not separable in the impedance spectrum. Both capacitive and resistive behaviors of the equivalent-circuit element could stem from either the grains or the grain boundaries or a mixture of both.

Figure 5 summarizes the differences between the equivalent circuit to represent a thick-ceramic sample and a thin-film sample and their origins. As can be seen from the sketch, with decreasing film thickness and grain size of the thin films, the interface becomes more important. The same applies to both capacitive and resistive contributions of the grain boundaries compared to the grains because they account for a higher fraction of the lateral film area (normal to the applied field direction).

APPENDIX D: COMPLIANCE WITH KRAMERS-KRONIG RELATION

Impedance spectra might be afflicted with artifacts. To identify artifacts and reconstruct artifact-free (or
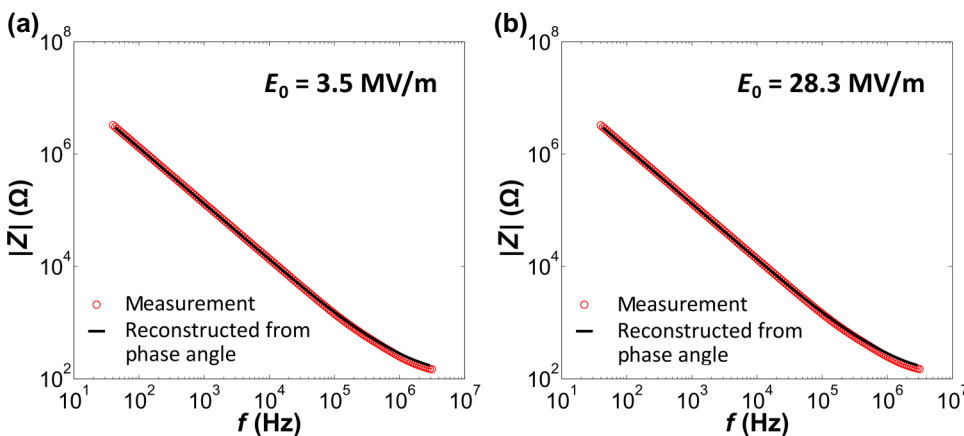

FIG. 6. Comparison of measured and reconstructed impedance Z for (a) $E_0 = 3.5$ MV/m and (b) $E_0 = 28.3$ MV/m, i.e., excitation fields below and beyond the threshold field. A good agreement is obtained for the range where the Rayleigh element is fitted to the data. Discrepancies arise in the higher frequency range where the interfacial layer and imperfect electrodes dominate.

less-artifact-afflicted) spectra, approaches based on the KK relations are used [67–70]. The standard equivalent-circuit elements (resistor, capacitor, inductor, and also the constant-phase element) and combinations of them imply that the represented system is stable, causal, linear, and exhibits finite values over the entire frequency range and thus, fulfills the KK relation. Here, the so-called Z-HIT (the two-pole Hilbert transform) as introduced by Schiller *et al.* [70] was used.

As can be seen from Fig. 1 in the main document, the Rayleigh law implies the presence of a certain nonlinearity, which means that compliance with the KK relation is no prerequisite for the corresponding data sets obtained at ac excitation fields beyond the threshold field. However, it is shown later in Fig. 3 that this nonlinearity is comparably small. Figure 6 shows the measured absolute values of Z in comparison with their counterparts reconstructed from the less artifact-prone [70] phase angle curves. As can be seen, the measured and reconstructed curves match fairly well for both an excitation field amplitude below and beyond the threshold field of about 10 MV/m as obtained from Fig. 3. This is believed to be due to the aforementioned small nonlinearity in the present sample. For higher frequencies of around 1 MHz, deviations increase. This is the range where the interfacial layer and imperfect electrodes dominate the equivalent circuit. However, this range is not of central interest for the fit of the Rayleigh element introduced in this work. Nonetheless, it once again emphasizes that caution is warranted when choosing the measurement frequency for a single-frequency approach.

[1] Premi Chandra and Peter B. Littlewood, A Landau Primer for Ferroelectrics, in *Physics of Ferroelectrics: A Modern Perspective, Number 105 in Topics Appl. Physics*, edited by K. Rabe, C. H. Ahn, and J.-M. Triscone (Springer-Verlag, Berlin, Heidelberg, 2007), pp. 69–116.

[2] L. E. Cross, Relaxorferroelectrics: An overview, Ferroelectrics **151**, 305 (1994).

[3] D. Damjanovic, Ferroelectric, dielectric and piezoelectric properties of ferroelectric thin films and ceramics, Rep. Prog. Phys. **61**, 1267 (1998).

[4] Lord Rayleigh, XXV. Notes on electricity and magnetism.—III. On the behaviour of iron and steel under the operation of feeble magnetic forces, London Edinb. Dublin Philos. Mag. J. Sci. **23**, 225 (1887).

[5] D. A. Hall, Rayleigh behaviour and the threshold field in ferroelectric ceramics, Ferroelectrics **223**, 319 (1999).

[6] D. A. Hall and P. J. Stevenson, High field dielectric behaviour of ferroelectric ceramics, Ferroelectrics **228**, 139 (1999).

[7] H. Dederichs and G. Arlt, Aging of Fe-doped PZT ceramics and the domain wall contribution to the dielectric constant, Ferroelectrics **68**, 281 (1986).

[8] D. V. Taylor and D. Damjanovic, Evidence of domain wall contribution to the dielectric permittivity in PZT thin films at sub-switching fields, J. Appl. Phys. **82**, 1973 (1997).

[9] H. Kronmüller, Statistical theory of Rayleigh's law, Z. Angew. Phys. **30**, 1 (1970).

[10] O. Boser, Statistical theory of hysteresis in ferroelectric materials, J. Appl. Phys. **62**, 1344 (1987).

[11] T. Nattermann, Y. Shapir, and I. Vilfan, Interface pinning and dynamics in random systems, Phys. Rev. B **42**, 8577 (1990).

[12] L. Néel, Théories des lois d'aimantation de Lord Rayleigh, Cah. Phys. **12**, 1 (1942).

[13] F. Preisach, Über die magnetische Nachwirkung, Z. Phys. **94**, 277 (1935).

[14] S. S. N. Bharadwaja, A. Laha, S. Halder, and S. B. Krupanidhi, Reversible and irreversible switching processes in pure and lanthanum modified lead zirconate thin films, Mater. Sci. Eng. B **94**, 218 (2002).

[15] Z. Luo, X. Lou, F. Zhang, Y. Liu, D. Chang, C. Liu, Q. Liu, B. Dkhil, M. Zhang, X. Ren, and H. He, Rayleigh-like nonlinear dielectric response and its evolution during electrical fatigue in antiferroelectric $(Pb, La)(Zr, Ti)O_3$ thin film, Appl. Phys. Lett. **104**, 142904 (2014).

[16] U. Böttger, Dielectric Properties of Polar Oxides, in *Polar Oxides: Properties, Characterization, and Imaging*, edited by R. Waser, U. Böttger, and S. Tiedke (Wiley-VCH Verlag GmbH & Co. KGaA, Weinheim, 2006).

[17] E. Barsoukov and J. R. Macdonald, *Impedance Spectroscopy: Theory, Experiment, and Applications* (John Wiley & Sons, Inc., Hoboken, NJ, USA, 2005).

[18] E. D. Grimley, T. Schenk, X. Sang, M. Pešić, U. Schroeder, T. Mikolajick, and J. M. LeBeau, Structural changes underlying field-cycling phenomena in ferroelectric HfO_2 thin films, Adv. Electron. Mater. **2**, 1600173 (2016).

[19] J. T. S. Irvine, D. C. Sinclair, and A. R. West, Electroceramics: Characterization by impedance spectroscopy, Adv. Mater. **2**, 132 (1990).

[20] C.-H. Kim, S.-I. Pyun, and J.-H. Kim, An investigation of the capacitance dispersion on the fractal carbon electrode with edge and basal orientations, Electrochim. Acta **48**, 3455 (2003).

[21] J.-B. Jorcin, M. E. Orazem, N. Pébère, and B. Tribollet, CPE analysis by local electrochemical impedance spectroscopy, Electrochim. Acta **51**, 1473 (2006).

[22] B. Hirschorn, M. E. Orazem, B. Tribollet, V. Vivier, I. Frateur, and M. Musiani, Constant-phase-element behavior caused by resistivity distributions in films I. Theory, J. Electrochem. Soc. **157**, C452 (2010).

[23] B. Hirschorn, M. E. Orazem, B. Tribollet, V. Vivier, I. Frateur, and M. Musiani, Constant-phase-element behavior caused by resistivity distributions in films II. Applications, J. Electrochem. Soc. **157**, C458 (2010).

[24] M. Musiani, M. E. Orazem, N. Pébère, B. Tribollet, and V. Vivier, Constant-phase-element behavior caused by coupled resistivity and permittivity distributions in films, J. Electrochem. Soc. **158**, C424 (2011).

[25] M. E. Orazem, I. Frateur, B. Tribollet, V. Vivier, S. Marcelin, N. Pébère, A. L. Bunge, E. A. White, D. P. Riemer, and M. Musiani, Dielectric properties of materials showing constant-phase-element (CPE) impedance response, J. Electrochem. Soc. **160**, C215 (2013).

[26] D. V. Taylor and D. Damjanovic, Domain wall pinning contribution to the nonlinear dielectric permittivity in $Pb(Zr, Ti)O_3$ thin films, Appl. Phys. Lett. **73,** 2045 (1998).

[27] U. Robels, Ch. Zadon, and G. Arlt, DiP219: Linearization of dielectric nonlinearity by internal bias fields, Ferroelectrics **133,** 163 (1992).

[28] C. Borderon, R. Renoud, M. Ragheb, and H. W. Gundel, Dielectric long time relaxation of domains walls in $PbZrTiO_3$ thin films, Appl. Phys. Lett. **104,** 072902 (2014).

[29] S. Bhaskar, S. B. Majumder, R. R. Das, P. S. Dobal, R. S. Katiyar, and S. B. Krupanidhi, Electrical properties of La-graded heterostructure of $Pb_{1-x}La_xTiO_3$ thin films, Mater. Sci. Eng. **B86,** 172 (2001).

[30] D. A. Hall, Review Nonlinearity in piezoelectric ceramics, J. Mater. Sci. **36,** 4575 (2001).

[31] S. S. N. Bharadwaja, D. Damjanovic, and N. Setter, Analysis of the non linear domain wall response in ferroelectric thin films, Ferroelectrics **303,** 59 (2004).

[32] C. Richter, T. Schenk, M. H. Park, F. A. Tscharntke, E. D. Grimley, J. M. LeBeau, C. Zhou, C. M. Fancher, J. L. Jones, T. Mikolajick, and U. Schroeder, Si doped hafnium oxide—A "fragile" ferroelectric system, Adv. Electron. Mater. **3,** 1700131 (2017).

[33] Jean-Luc Dellis, Zfit, version 1.2 (downloaded 2017-05-15), https://www.mathworks.com/matlabcentral/fileexchange/19460-zfit

[34] See Supplemental Material at http://link.aps.org/supplemental/10.1103/PhysRevApplied.10.064004 for all impedance fits of the different AC excitation field amplitudes, an complementary plot for Rayleigh analysis and Rayleigh plots obtained from a conventional single-frequency approach.

[35] Y. Guan, D. Zhou, J. Xu, X. Liu, F. Cao, X. Dong, J. Müller, T. Schenk, and U. Schroeder, The Rayleigh law in silicon doped hafnium oxide ferroelectric thin films, Phys. Status Solidi RRL **9,** 589 (2015).

[36] N. Bassiri-Gharb, I. Fujii, E. Hong, S. Trolier-McKinstry, D. V. Taylor, and D. Damjanovic, Domain wall contributions to the properties of piezoelectric thin films, J. Electroceram. **19,** 49 (2007).

[37] D. Bolten, U. Böttger, T. Schneller, M. Grossmann, O. Lohse, and R. Waser, Reversible and irreversible processes in donor-doped $Pb(Zr, Ti)O_3$, Appl. Phys. Lett. **77,** 3830 (2000).

[38] E. D. Grimley, T. Schenk, T. Mikolajick, U. Schroeder, and J. M. LeBeau, Atomic structure of domain and interphase boundaries in ferroelectric HfO_2, Adv. Mater. Interfaces **5,** 1701258 (2018).

[39] P. Buragohain, C. Richter, T. Schenk, H. Lu, U. Schroeder, and A. Gruverman, Nanoscopic studies of domain structure dynamics in ferroelectric La : HfO_2 capacitors, Appl. Phys. Lett. **112,** 222901 (2018).

[40] D. A. Hall, P. J. Stevenson, and S. W. Mahon, The effect of static compressive stress on the high field dielectric properties of hard PZT ceramics, in *Piezoelectric Materials: Advances in Science, Technology and Applications*, edited by C. Galassi, M. Dinescu, K. Uchino, and M. Sayer (Springer, Dordrecht, 2000), pp. 149–157.

[41] T. Schenk, M. Hoffmann, J. Ocker, M. Pešić, T. Mikolajick, and U. Schroeder, Complex internal bias fields in ferroelectric hafnium oxide, ACS Appl. Mater. Interfaces **7,** 20224 (2015).

[42] U. Schroeder, C. Richter, M. H. Park, T. Schenk, M. Pešić, M. Hoffmann, F. P. G. Fengler, D. Pohl, B. Rellinghaus, C. Zhou, C.-C. Chung, J. L. Jones, and T. Mikolajick, Lanthanum-doped hafnium oxide: A robust ferroelectric material, Inorg. Chem. **57,** 2752 (2018).

[43] T. Schenk, PhD thesis: TU Dresden, 2016.

[44] U. Schroeder, M. Pešic, T. Schenk et al., in *Proceedings of the 46th IEEE European Solid-State Device Research Conference (ESSDERC)*, Lausanne, (2016), pp. 364–368.

[45] R. Materlik, C. Künneth, and A. Kersch, The origin of ferroelectricity in $Hf_{1-x}Zr_xO_2$: A computational investigation and a surface energy model, J. Appl. Phys. **117,** 134109 (2015).

[46] M. Hoffmann, T. Schenk, M. Pešić, U. Schroeder, and T. Mikolajick, Insights into antiferroelectrics from first-order reversal curves, Appl. Phys. Lett. **111,** 182902 (2018).

[47] M. Pešić, M. Hoffmann, C. Richter, S. Slesazeck, T. Kämpfe, L. M. Eng, T. Mikolajick, and U. Schroeder, in Proceedings of the 47th IEEE European Solid-State Device Research Conference (ESSDERC), Leuven (2017), pp. 160-163.

[48] M. Pešić, M. Hoffmann, C. Richter, T. Mikolajick, and U. Schroeder, Physical mechanisms behind the field-cycling behavior of HfO_2-based ferroelectric capacitors, Adv. Funct. Mater. **26,** 7486 (2016).

[49] J. F. Scott, There's no place like Ohm: Conduction in oxide thin films, J. Phys.: Condens. Matter. **26,** 142202 (2014).

[50] F.-C. Chiu, A review on conduction mechanisms in dielectric films, Adv. Mater. Sci. Eng. **2014,** 578168 (2014).

[51] G. Kirchhoff, Ueber den Durchgang eines elektrischen Stromes durch eine Ebene, insbesondere durch eine kreisförmige, Ann. Phys. **40,** 497 (1845).

[52] J. C. Maxwell, A dynamical theory of the electromagnetic field, Phil. Trans. R. Soc. Lond. **155,** 459 (1865).

[53] F. J. Dyson, Feynman's proof of the Maxwell equations, Am. J. Phys. **58,** 209 (1990).

[54] S. Tiedke and T. Schmitz, Electrical characterization of nanoscale ferroelectric structures, in *Nanoscale Characterisation of Ferroelectric Materials*, edited by M. Alexe and A. Gruverman (Springer, Berlin, Heidelberg, 2004).

[55] K. M. Rabe, C. H. Ahn, and J.-M. Triscone, *Physics of Ferroelectrics: A Modern Perspective* (Springer Publishing Company, Berlin Heidelberg, 2007).

[56] A. K. Jonscher, The "universal" dielectric response, Nature **267,** 673 (1977).

[57] A. K. Jonscher, The universal dielectric response and its physical significance, IEEE Trans. Electr. Insul. **27,** 407 (1992).

[58] A. K. Jonscher, Dielectric relaxation in solids, J. Phys. D: Appl. Phys. **32,** R57 (1999).

[59] A. K. Jonscher, Energy criterion in the interpretation of dielectric relaxation, Appl. Phys. A **56,** 405 (1993).

[60] J. R. Macdonald, Comparison of the universal dynamic response power-law fitting model for conducting systems with superior alternative models, Solid State Ion. **133,** 79 (2000).

[61] D. A. Hall, M. M. Ben-Omran, and P. J. Stevenson, Field and temperature dependence of dielectric properties in-based piezoceramics, J. Phys.: Condens. Matter. **10,** 461 (1998).

[62] G. Robert, D. Damjanovic, and N. Setter, Preisach modeling of ferroelectric pinched loops, Appl. Phys. Lett. **77,** 4413 (2000).

[63] T. Schenk, E. Yurchuk, S. Mueller, U. Schroeder, S. Starschich, U. Böttger, and T. Mikolajick, About the deformation of ferroelectric hystereses, Appl. Phys. Rev. **1,** 041103 (2014).

[64] M. Hoffmann, U. Schroeder, T. Schenk, T. Shimizu, H. Funakubo, O. Sakata, D. Pohl, M. Drescher, C. Adelmann, R. Materlik, A. Kersch, and T. Mikolajick, Stabilizing the ferroelectric phase in doped hafnium oxide, J. Appl. Phys. **118,** 072006 (2015).

[65] V. Iglesias Santiso, PhD thesis: Universitat Autònoma de Barcelona, 2013.

[66] D. Martin, M. Grube, W. Weinreich, J. Müller, W. M. Weber, U. Schröder, H. Riechert, and T. Mikolajick, Mesoscopic analysis of leakage current suppression in $ZrO_2/Al_2O_3/ZrO_2$ nano-laminates, J. Appl. Phys. **113,** 194103 (2013).

[67] M. Urquidi-Macdonald, S. Real, and D. D. Macdonald, Applications of Kramers—Kronig transforms in the analysis of electrochemical impedance data—III. Stability and linearity, Electrochim. Acta **35,** 1559 (1990).

[68] B. A. Boukamp, A linear Kronig-Kramers transform test for immittance data validation, J. Electrochem. Soc. **142,** 1885 (1995).

[69] P. Agarwal, M. E. Orazem, and L. H. Garcia-Rubio, Application of measurement models to impedance spectroscopy III. Evaluation of consistency with the Kramers-Kronig relations, J. Electrochem. Soc. **142,** 4159 (1995).

[70] C. A. Schiller, F. Richter, E. Gülzow, and N. Wagner, Validation and evaluation of electrochemical impedance spectra of systems with states that change with time, Phys. Chem. Chem. Phys. **3,** 374 (2001).